

DW Cancri in x-rays

A.A. Nucita,^{1,2★} L. Conversi,³ D. Licchelli,⁴

¹ *Department of Mathematics and Physics “E. De Giorgi”, University of Salento, Via per Arnesano, CP-193, I-73100, Lecce, Italy*

² *INFN, Sezione di Lecce, Via per Arnesano, CP-193, I-73100, Lecce, Italy*

³ *Euclid Science Operation Centre, European Space Astronomy Centre, European Space Agency, P.O. Box 78 - 28691, Villanueva de la Canada, (Madrid) - Spain*

⁴ *R.P. Feynman Observatory, Gagliano del Capo, I-73034 Lecce, Italy and CBA, Center for Backyard Astrophysics - Gagliano del Capo, I-73034, Lecce, Italy*

Accepted XXX. Received YYY; in original form ZZZ

ABSTRACT

We report on the *XMM*-Newton observation of DW Cnc, a candidate intermediate polar candidate whose historical optical light curve shows the existence of periods at ≈ 38 , ≈ 86 and ≈ 69 minutes which were interpreted as the white dwarf spin, the orbital and the spin-orbit beat periodicities. By studying the 0.3–10 keV light curves, we confirm the existence of a period at ≈ 38 minutes and find in the OM light curve a signature for a period at 75 ± 21 minutes which is consistent with both the orbital and spin-orbit beat. These findings allow us to unveil without any doubt, the nature of DW Cnc as an accreting intermediate polar. The EPIC and RGS source spectra were analyzed and a best fit model, consisting of a multi-temperature plasma, was found. The maximum temperature found when fitting the data is $kT_{max} \approx 31$ keV which can be interpreted as an upper limit to the temperature of the shock.

Key words: (stars:) novae, cataclysmic variables; X-rays: binaries; X-rays: individual: DW Cancri; (stars:) white dwarfs

1 INTRODUCTION

Cataclysmic variables (CVs) are binary systems with a white dwarf (WD) primary star accreting material from a donor (secondary) companion. Although the two stars interact principally via the formation of a Roche-lobe (see, e.g. Kuulkers et al. 2006 for a review), the accretion depends on several parameters as the strength of the magnetic field. In fact, depending on its value, CVs can be classified in non-magnetic systems, characterized by a weak field ($\lesssim 0.1$ MG) and an accretion disk and, possibly, a boundary layer around the primary (see, e.g., van Teeseling et al. 1996; Nucita et al. 2009 a; Hoard et al. 2010; Nucita et al. 2009 b, 2011; Balman 2011; Nucita et al. 2014; Mukai et al. 2017 to cite a few); intermediate polars (with magnetic field in the range 0.1–10 MG) where the accretion disk is partially disrupted close the central white dwarf (see, e.g. Haberl 2002; Evans & Hellier 2004 a; Evans et al. 2004 b; Evans & Hellier 2005; Evans et al. 2006; Evans & Hellier 2007; de Martino et al. 2004, 2005; Mukai et al. 2015; Bernardini et al. 2017); and polars (see, e.g., Ramsay et al. 2004; Szkody et al. 2004) consisting of highly magnetized

objects ($\gtrsim 10$ MG) in which the accretion occurs via a mass flow directly pushed onto the white dwarf poles.

In intermediate polars and polars the accretion flow (driven by the magnetic field) undergoes a strong shock close to the WD and releases X-rays to optical emission. Since the magnetic axis is offset from the WD spin one, the observed signal may show a modulation at the spin period and, in some cases, at lower time-scales depending whether parts of both poles are visible. Sometimes, a modulation in the X-rays light curves on the time scale of the orbital period is also observed (Parker et al. 2005). These pulsations may be caused by a dependence of the accretion region view on the binary phase.

Another possibility could be the existence of a second emission component (caused by the interaction of the mass flow with an accretion disk or the white dwarf magnetosphere) whose visibility changes with time. In alternative, if a non-axisymmetric disk exists, X-rays could suffer of a local absorption when the line of sight intersects the absorption structures. In the latter case, one would expect a decreasing of the modulation depth with increasing X-ray energy, thus suggesting photoelectric absorption as the main cause.

In this respect, DW Cancri (hereafter DW Cnc) is a variable binary identified as a CV from its Balmer emission lines (Stepanian 1982; Kopylov et al. 1988). Uemura

★ E-mail: nucita@le.infn.it

(2002) reported kilosecond quasiperiodic oscillations (37 and 73 minutes) in the light curve, while [Rodríguez-Gil et al. \(2004\)](#), by performing radial velocity measurements, showed the existence of a period in the range 77–86 minutes. Finally, [Patterson et al. \(2004\)](#) reported the results of photometric and spectroscopic observations of the target. In particular, strong detection of the periods $\approx 86.1015(3)$ minutes and $38.58377(6)$ minutes were derived from radial-velocity measurements and interpreted as, respectively, the orbital period P_{orb} of the binary (so that DW Cnc is a candidate CV below the period gap) and the spin period P_{spin} of a magnetic white dwarf. Further analysis on the DW Cnc light curve also showed the existence of a strong signal at spin $69.9133(10)$ minutes coinciding with the difference frequency $2\pi/P_{spin} - 2\pi/P_{orb}$.

[Patterson et al. \(2004\)](#) also pointed out that the detected periods are stable at least over one year and, since the observed light curve resembles the behaviour of several members of the DQ Herculis sub-class of CV (i.e. intermediate polar), DW Cnc might be considered as an intermediate polar CV as well. As noted by [Patterson et al. \(2004\)](#) (but see also [Mukai 2005](#)), a high energy view of DW Cnc (with a confirmation of the pulse period) was lacking. This is of particular interest since the detection of any X-ray pulsation at the white dwarf rotational period could be described in the framework of the model accretion model proposed by [Hellier et al. \(1991\)](#) and would be the signature of a channelled accretion in DW Cnc.

Hence, we present a ≈ 9.4 ks *XMM-Newton* observation of the intermediate polar candidate DW Cnc showing that its spin pulse is clearly detected in the X-ray band thus unveiling its nature as a intermediate polar object. We then discuss the spectral and timing analysis conducted on data collected by the EPIC and RGS cameras and the OM telescope interpreting the observed properties as possibly due to changes of view of the X-ray emitting region.

2 XMM-NEWTON VIEW OF DW CANCRI

2.1 Data reduction

DW Cnc (with J2000 coordinates $RA = 07^h58^m53.10^s$ and $DEC = +16^\circ16'45.1''$) was observed by the *XMM-Newton* satellite in 2012 (Observation ID 0673140101) for ≈ 9.4 ks during what appeared to be a normal quiescent state¹ of the target. The observation started (ended) on 2012/04/02 at 09 : 06 : 03 (11 : 43 : 04) UT with the EPIC pn (MOS) camera operating in large (small) window mode. The medium filter was selected during the observation. RGS 1 and 2 data were also available. The Optical Monitor (OM) aboard the satellite also observed the target in fast mode (thus allowing a time resolution of 0.5 seconds) and with the UVM2 filter centered at ≈ 231 nm.

The EPIC raw data files (ODFs) were processed using the *XMM-Science Analysis System* (SAS version 17.0.0). The data were processed using the latest available calibration constituent files (CCFs) and the event lists for the three

EPIC cameras obtained by running the *emchain* and *epchain* task, thus producing calibrated event files. We then searched for segments of the observation affected by soft proton flares and determined a list of good time intervals through which cleaned event files (suitable for the following analysis) were produced. The files were also corrected for the barycenter (via the *barycen* SAS tool) so that the photon arrival times are in the barycentric dynamical time instead of spacecraft time.

The source (plus background) signals in the soft (0.3–2 keV), hard (2–10 keV) and full (0.3–10 keV) bands were extracted from circular regions centered on the nominal DW Cnc coordinates and with radii of $40''$ thus allowing a collection of $\approx 88\%$ of the total energy. The background counts were extracted (for the same energy bands as above) from surrounding circular regions with radii of $115''$. For each EPIC camera and energy band, we produced synchronized source (plus background) and background light curves with bin size of 10 seconds. The background light curves were then scaled (mainly accounting for the source extraction area) and subtracted from the source light curves by using the *epicccorr* task. Note that the soft, hard and full X-ray light curves were also synchronized to each other so that they can be combined thus increasing the signal-to-noise ratio. As a result of the above procedure the EPIC soft, hard and full (background corrected) light curves started (ended) at $MJD = 56019.40173$ ($MJD = 56019.48471$) and correspond to average count rate of 2.2 ± 0.5 , 0.7 ± 0.5 , and 2.9 ± 0.7 counts s^{-1} , respectively. The soft, hard and full X-ray light curves are shown (from top to bottom) in the left panels of Figure 1.

The OM UVM2 data were extracted by using the standard *omfchain* task with time resolution set to 10 seconds. This resulted in a count rate light curve that was corrected for the solar system barycenter and converted into magnitude assuming a zero point of ≈ 15.77 . Hence the baseline magnitude (see also Figure 3 where the start of the observation corresponds to $MJD = 56019.38789$) is 13.93 ± 0.25 during the *XMM-Newton* observation. As one can note, the OM observation (lasting for ≈ 146.6 minutes) is characterized by a small gap (≈ 318 seconds) as the the maximum allowed integration time for an exposure in fast mode is ≈ 4.4 ks.

As far as the spectral data is concerned, the EPIC source and background spectra were extracted in the same regions as above. Furthermore, high resolution spectra from the RGS1 and RGS2 cameras were obtained (together with the corresponding ancillary files) by running SAS task *rgsproc*. Then, the epic source (background corrected) spectra (one for each camera) was first re-binned to ensure that there were at least 25 counts per energy bin and then imported (together with all the relevant quantities as the response matrix and ancillary file) within the XSPEC package (version 12.9.0) for the spectral analysis and fitting procedure (see Section 2.3).

2.2 Timing analysis

As described in the previous section, the barycentric/background corrected light curves (lasting for ≈ 119.5 minutes) were extracted in the soft (0.3–2 keV) and hard (2–10 keV) bands with a bin size of 10 seconds. The X-ray light curves and the associated hardness ratio were used to

¹ The historical AAVSO (The American Association of Variable Star Observers, <https://www.aavso.org/>) shows that DW Cnc is stable on a baseline of several years.

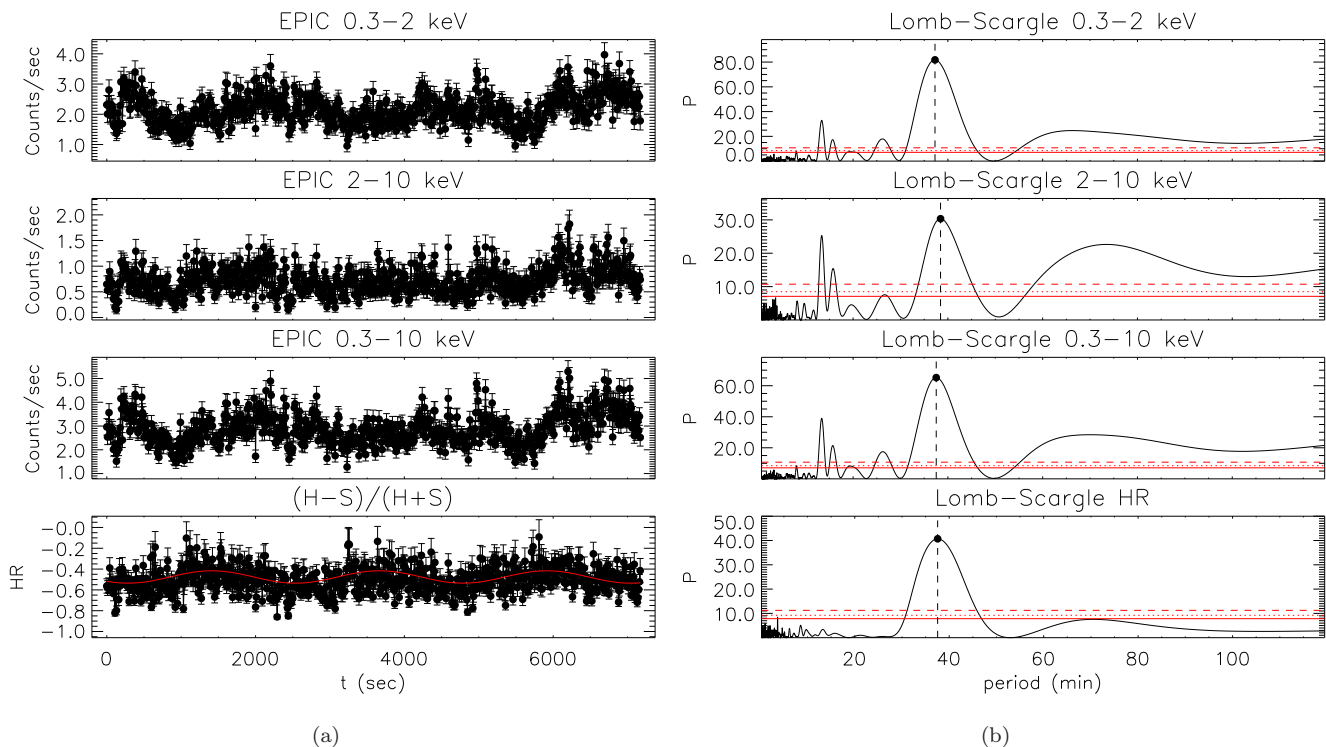


Figure 1. Left panel: the DW Cnc Epic (background subtracted and synchronized) light curves in the 0.3–2 keV, 2–10 keV and 0.3–10 keV bands and the hardness ratio together with the best fit sinusoidal function, respectively. Each light curve has a bin size of 10 seconds and the start of the observation corresponds to MJD = 56019.40173 days. Right panel: the associated Lomb-Scargle periodograms with the identification of the WD spin period.

perform a blind search for periodicities in the range between twice the bin size and half the observational window with the well-known Lomb-Scargle technique (Scargle 1982). This search resulted in the identification of a periodic feature as indicated by the dashed vertical lines in the left panels of Figure 1, being the red horizontal lines the false alarm probability thresholds at 68% (solid), 90% (dotted), and 99% (dashed) level, respectively. The average position of the feature corresponds to the periodicity of 37.7 ± 4.5 minutes, i.e. consistent with spin period (P_{spin}) of the white dwarf already identified by Uemura (2002) and Patterson et al. (2004), thus confirming this signature in the high energy data from DW Cnc. Note that the duration of the X-ray light curve limits our capability in any clear detection via the Lomb-Scargle periodogram technique of the orbital period (expected to be at ≈ 86 minutes) nor the periodicity associated to the difference frequency ($\omega_{spin} - \omega_{orb} = 2\pi/P_{spin} - 2\pi/P_{orb}$) at ≈ 69 minutes. This is also confirmed when using other analysis tools as the epoch folding technique. We also point to the fact that the timing analysis reveals powers at harmonics of the white dwarf period as, in particular, $P_{spin}/2 \approx 19$ minutes (although at a low confidence level) and $P_{spin}/3 \approx 14$ minutes. More interestingly, we noted in the power spectrum (see Figure 1) the existence of a peak at ≈ 26 minutes which resembles the side-band feature ($\omega_{spin} + \omega_{orb} = 2\pi/P_{spin} + 2\pi/P_{orb}$) expected from $2\omega_{orb}$ modulation (see, e.g., Norton et al. 1996).

We folded the soft, hard and full light curves at the

white dwarf spin period (see Figure 2) using 50 bins and note that the data show a quasi-sinusoidal behaviour with a broad maximum. In order to evaluate the degree of X-ray spin modulation, we define the percentage fractional modulation as $100 \cdot (M - m)/M$ where M and m are the maximum and minimum flux in the binned (both soft and hard) light curves. This resulted in fractional modulations resulted to be $43 \pm 4\%$ (soft band) and $48 \pm 5\%$ (hard band), respectively. The general smooth and nearly sinusoidal light curves observed in different bands (2) and the fact that the soft and hard fractional modulations are consistent within the quoted errors, possibly imply that the rotational pulses could have their origin in the aspect changes (i.e. occultations) of the X-ray emitting region (a polar cap) as the WD rotates².

Note however that the hardness ratio curve is characterized by a modulation with the white dwarf spin period. This is clear from the bottom panel in Figure 1 where, as usual, we define the hardness ratio HR as $HR = (H - S)/(H + S)$, where S and H represents the count rates in the soft and hard bands, respectively. Inspection of this figure shows that the hardness ratio remains negative (due to an average emission in the soft band larger than the harder one) and has a sinusoidal behaviour as shown by the best fit sinusoidal

² Furthermore, since the X-ray source never suffers of complete occultations (and no important spectral changes are observed, see Section 2.3) implies that the oblique rotator is observed at low inclination.

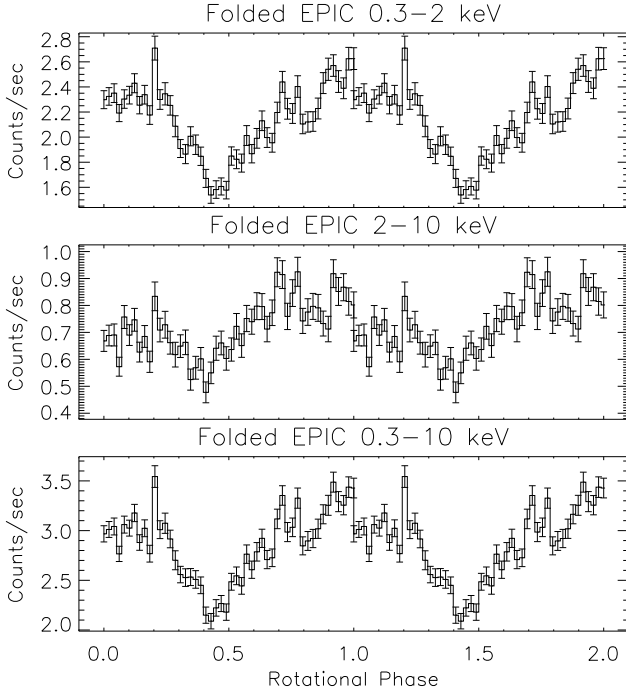


Figure 2. The EPIC light soft, hard and full curves folded in 50 bins (each corresponding to ≈ 45.04 s) at the spin period of the white dwarf.

function (obtained fixing the period to that derived by the Lomb-Scargle periodogram) superimposed to the data. This behaviour could arise (in part or totally) from the existence of a complex, partial covering absorption column as observed in other intermediate polars. We investigate this issue in Section 2.3 by performing a phase resolved spectral analysis.

The OM data in the UVM2 filter covers a total length of ≈ 146.6 minutes so that one could in principle detect any feature (if present) with periodicity of $\approx 69 - 86$ minutes as these signal would be present with at least ≈ 2 full cycles. The periodicity was searched for by constructing the corresponding Lomb-Scargle periodogram³. This procedure resulted in a clear identification in the optical data of a period of 75 ± 21 minutes which, within the quoted errors, is consistent with both the 69 and 86 minute features previously reported. The large error is due to the peak broadening in the associated periodogram.

³ We note here that, as discussed in Belanger (2016), the presence of gaps in the data introduces structures in the periodogram (including the Lomb-Scargle one) and, in particular, a sort of reddening effect appears. Hence, we filled the OM gap by randomly selecting data points from the remaining part of the light curve thus preserving the overall characteristics as bin size, *rms* and noise of the data. For each light curve, the periodicity was searched for by constructing the corresponding Lomb-Scargle periodogram and the results averaged.

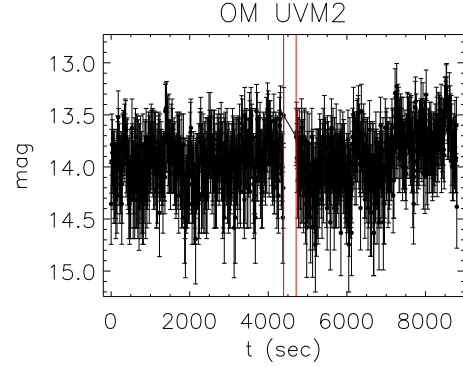


Figure 3. The OM light curve (in the UVM2 filter centered at 231 nm) is shown with a bin size of 10 seconds. The start of the observation corresponds to MJD = 56019.38789 days with the full light curve lasting for ≈ 2.44 hours.

2.3 Spectral analysis

We first simultaneously fit the background subtracted MOS 1, MOS 2 and pn spectra (grouped on a minimum of 25 counts per energy channel) with a simple bremsstrahlung model absorbed by a neutral hydrogen foreground column and a constant of proportionality to account for any possible difference between the detector responses (within XSPEC the model is *const * phabs * brems*). We fixed the hydrogen column density to the average value found in the direction of the target ($nH = 3.52 \times 10^{20} \text{ cm}^{-2}$ Kalberla et al. 2005). The resulting fit quality is very poor ($\chi^2 = 4.05$ for 542 degrees of freedom, d.o.f.) and large residuals appear in the energy range 0.7 – 1 keV (possibly due to the blended-iron L-shell complex around 1 keV) and at the K line locations of heavy elements, in particular the features at 6.65 and 6.69 keV, plus residuals corresponding to the fluorescence of iron at 6.4 keV. In this respect, when repeating the analysis by adding three thin Gaussian lines (at 6.4, 6.65, and 6.69 keV) and one broad Gaussian centered at ≈ 0.8 keV the quality of the fit dramatically improves ($\chi^2 = 1.32$ for 535 d.o.f.) but still remaining statistically unacceptable.

These results led us to examine the spectrum with an emission model (as *mekal*, Mewe et al. 1985) of hot plasma in collisional ionization equilibrium able to simulate line emissions from different elements. A single temperature model (*const * phabs * mekal* in XSPEC), with hydrogen column density as above and metal abundances set to the solar ones) resulted in plasma temperature of ≈ 5.3 keV but very poor from the statistical point of view ($\chi^2 = 4.83$ for 543 d.o.f.). Since, relaxing the assumption of the solar abundance did not improve the fit, this is an hint that a multi-temperature plasma is acting. We found a reasonable fit by requiring a three component plasma ($\chi^2 = 1.05$ for 538 d.o.f.) with temperatures $kT_1 = 11.4^{+2.0}_{-2.0}$ keV, $kT_2 = 1.3^{+0.1}_{-0.1}$ keV, and $kT_3 = 0.60^{+0.10}_{-0.10}$ keV, respectively. The metal abundance converged towards the value $A_Z = 0.42 \pm 0.10$. All the errors (here and hereinafter are quoted at the 90% confidence level).

Apart from small residuals around the iron complex lines, we note that an excess below 0.4 keV is still present. This excess is accounted for when we relaxed the value of the hydrogen column density so that the fit converged towards ($\chi^2 = 0.97$ for 537 d.o.f.) a three plasma model with metal

abundance of $A_Z = 0.66 \pm 0.10$, temperatures $kT_1 = 11.7^{+2.0}_{-1.0}$ keV, $kT_2 = 1.3^{+0.1}_{-0.1}$ keV, and $kT_3 = 0.61^{+0.04}_{-0.04}$ keV and neutral hydrogen column density $nH = (1.9 \pm 0.4) \times 10^{20} \text{ cm}^{-2}$. Note that the two previous models converge practically to the same values of temperatures (within the errors) regardless if the hydrogen column density is considered as a free fit parameter or fixed at its average galactic value observed towards the target.

In the previous Section, we showed that the hardness ratio light curve is characterized by a modulation with the white dwarf spin period. Since most of the IP are characterized by strong and very complex absorption (see, e.g. Mukai et al. 1994), the observed modulation could be explained by a partial covering absorption column.

To test this hypothesis, we fit the data using, as above, three mekal components with equal abundances and absorbed by both simple and partial absorptions, i.e. *const * phabs * pcfabs * (mekal + mekal + mekal)* in XSPEC. The best fit resulted in a metal abundance of $A_Z = 0.53^{+0.12}_{-0.09}$, temperatures $kT_1 = 10.5^{+1.2}_{-1.3}$ keV, $kT_2 = 1.4^{+0.1}_{-0.1}$ keV, and $kT_3 = 0.62^{+0.04}_{-0.05}$ keV, neutral hydrogen column density $nH = (2.2 \pm 0.5) \times 10^{20} \text{ cm}^{-2}$, complex equivalent hydrogen column $nH = (10.4^{+21.7}_{-9.1}) \times 10^{22} \text{ cm}^{-2}$ (being this value similar -although with large uncertainties - to column density values found in other IP objects, see e.g. Evans et al. 2006) and with a partial dimensionless covering factor $f = 0.11 \pm 0.08$.

Note that, although all the values of the interesting parameters remain practically unchanged with respect to the previous model, the associated χ^2 statistics ($\chi^2 = 0.97$ for 535 d.o.f.) and its negligible improvement does not justify the introduction of any complex partial covering thus favouring galactic absorption.

We further noted that the metal abundance sets to a relatively low value and, in addition, the simple three temperature plasma model (with all the parameters fixed to their best fit values except for the normalization constants) does not adapt to the RGS 1 and RGS 2 data failing in reproducing the overall shape and, in particular, the intensities of the transition lines as the He-like transitions of OVII (see Section 2.4). Hence, two possibilities are equally probable: the derived metal abundance is too low or a complex stratification of temperatures is required.

Observing that the accretion post shock regions are expected to have a gradient in temperature deriving from the cooling of the gas when falling onto the WD surface (de Martino et al. 2005), we used in XSPEC a multi-temperature scenario based on the *cemekl* model (still intrinsically dependent on *mekal*) absorbed by a neutral hydrogen distribution characterized by a column density. We remind that the *cemekl* model is normally used to account for a gradient of temperature in post-shock regions around CVs. In particular, the emission measure gradient follows a power law as $dEM/dT = (T/T_{max})^{\alpha-1}/T_{max}$. In this model, the free parameters are the neutral hydrogen column density, the maximum value of the plasma temperature T_{max} , the power law index α , the metal solar abundance A_Z relative to the solar one, the model normalization and a constant factor introduced for inter-calibration issues among the instruments. The best fit converged towards the values ($\chi^2 = 1.04$ for 540 d.o.f.) $nH = (3.1 \pm 0.3) \times 10^{20} \text{ cm}^{-2}$, $kT_{max} = 31^{+5}_{-4}$ keV, $\alpha = 0.65^{+0.06}_{-0.05}$, and $A_Z = 0.9^{+0.1}_{-0.1}$, respectively.

Table 1. Spectral parameters for the best fitting model (*const * phabs * (cemekl)* in XSPEC, see text for details). We also give the 0.3 – 10 keV absorbed and unabsorbed fluxes.

$nH = (3.1 \pm 0.3) \times 10^{20} \text{ cm}^{-2}$
$\alpha = (0.65^{+0.06}_{-0.05})$
$kT_{max} = 31^{+5}_{-4} \text{ keV}$
$A_Z = 0.9^{+0.1}_{-0.1}$
$F_{0.3-10\text{keV}}^{abs} = (1.59^{+0.02}_{-0.02}) \times 10^{-11} \text{ erg cm}^{-2} \text{ s}^{-1}$
$F_{0.3-10\text{keV}}^{una} = (1.68^{+0.02}_{-0.02}) \times 10^{-11} \text{ erg cm}^{-2} \text{ s}^{-1}$

Note that the low hydrogen column density of the absorber is consistent with the value of the galactic column density in the direction of the source so that, again, the introduction of any complex partial covering is not required. Differently to what happens in most of the observed IPs (Mukai et al. 1994), but in common with at least another IP object (HT Cam, de Martino et al. 2005), DW Cnc seems to be not characterized by complex local absorption, being this an hint that the X-ray source is not seen though any absorbing material (see also next) possibly in agreement with the fact that the soft and hard fractional modulations are consistent within the quoted errors.

As a by product, this model reproduces much better the overall structure of the RGS 1 and RGS 2 spectra (see Section 2.4) when fixing all the parameters to the best fit results and adjusting only the normalizations.

In order to investigate the white dwarf spin pulse profile and any possible dependence of the source spectral properties on the phase, we defined phase intervals (see Fig. 2) encompassing the regions around maxima (at phases 0-0.25 and 0.7-1) and minima (at phases 0.33-0.55) and extracted the corresponding spectra from the three XMM-Newton camera. The spectra were then fitted separately with the same model consisting in an absorbed multi-temperature plasma with all the interesting parameters free to vary but fixed metal abundance to the value obtained analyzing the phase averaged spectrum. As a result, we obtained $kT_{max} = 28^{+6}_{-4}$ keV and $\alpha = 0.57^{+0.06}_{-0.05}$, and $kT_{max} = 35^{+7}_{-8}$ keV and $\alpha = 0.61^{+0.10}_{-0.05}$ for maxima and minima, respectively. Clearly, at different phases, the spectral properties of the source are consistent within the quoted uncertainties.

The previous finding, and the fact that we do not find evidences for a local partial covering, pushes us in interpreting the observed variability due to aspect changes of the underlying X-ray emitting region as the WD rotates. In fact, in the scenario in which a polar cap never suffers of complete occultations (i.e. the oblique rotator is observed at a low inclination angle), changes in the observed projected area of the X-ray source naturally explains the observed modulation.

This model (see Figure 4) resulted in absorbed and unabsorbed 0.3 – 10 keV band fluxes of $F_{0.3-10\text{keV}}^{abs} = (1.59^{+0.02}_{-0.02}) \times 10^{-11} \text{ ergs}^{-1} \text{ cm}^{-2}$ and $F_{0.3-10\text{keV}}^{una} = (1.68^{+0.02}_{-0.02}) \times 10^{-11} \text{ ergs}^{-1} \text{ cm}^{-2}$, respectively, which correspond to luminosities of $\approx 8.2 \times 10^{31} \text{ ergs}^{-1}$ and $\approx 8.7 \times 10^{31} \text{ ergs}^{-1}$ when a distance of $\approx 208 \text{ pc}$ (as reported in the second Gaia data release, Brown et al. 2018) is assumed (see Table 1).

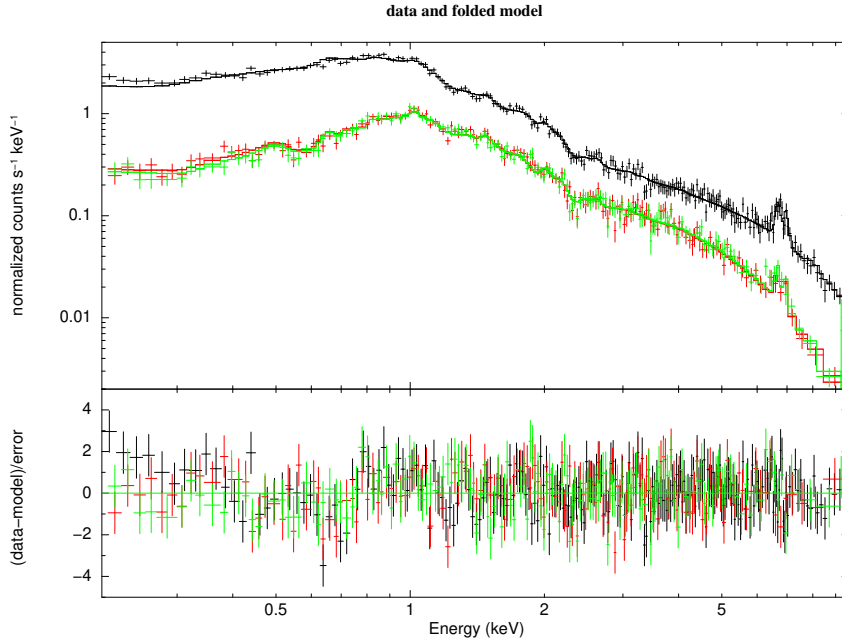


Figure 4. The best fit to the MOS 1, MOS 2, and pn data with the XSPEC model *const * phabs(cemekl)* (see text for details).

2.4 RGS data

Note that the same multi-temperature model used for the EPIC spectral fit provides an adequate description of the RGS spectra when fixing all the parameters of the model to those derived above but adjusting consistently the model normalizations. In particular, inspecting Figure 5 (where the best fit is superimposed to the RGS1 and RGS2 data rebinned in order to have at least a significance of 10σ per bin), one can note the existence of the OVIII Ly- α emission line at ≈ 0.65 keV, and emission lines in the energy range 0.56 keV–0.57 keV (21.6 Å–22.1 Å) possibly associated to the He-like transitions of OVII, i.e. the resonance line r (corresponding to the transitions between the $n = 2$ shell and the $n = 1$ ground state), and the inter-combination (i) and the forbidden (f) lines. In this respect, as shown by Porquet & Dubau (2000) the relative emission strength of the r , i and f lines is a good indicator of the physical conditions of density and temperature of the gas.

In order to have a measure of the line fluxes, we followed the phenomenological spectral analysis method described in Nucita et al. (2010) and references therein. In particular, the unbinned RGS spectra are divided in intervals of 100 channels wide and Gaussians are fitted to all the identified emission lines. For each (single) emission line the centroid energy is free to vary and, when triplets are identified, the relative distance between the central energies was frozen to the value predicted by atomic physics. The local continuum was always modelled as a power law with a fixed photon index $\Gamma = 1$ and normalization free to vary. Since we are dealing with the unbinned spectra, we estimated the goodness of the fit by using the C-statistic (see, Cash 1979). We further consider the line (or triplet) detected at 68% confidence level when, repeating the fit with the continuum only, we obtained a change in the C-statistic value (ΔC) by at least 2.3. The result of this analysis (see also Table 2) showed

that the OVII resonance line is much more weaker than the inter-combination line so that ionization processes may occur in the medium (Porquet & Dubau 2000). This is also clear when using the standard line ratios $R = f/i$, $L = r/i$, and $G = (f + i)/r$ as standard diagnostic. In particular, as clear from table 2, the large (small) values of the G (R) ratio imply photonionization and, since R decreases with increasing values of the electron density n_e , a lower limit on the electron density of $\approx 10^{11} \text{ cm}^{-3}$ (Porquet & Dubau 2000). Note also that the best fit line centroids seem to be shifted compared to the laboratory values by $-40^{+150}_{-190} \text{ km s}^{-1}$ for the OVIII Ly- α line and $440^{+260}_{-100} \text{ km s}^{-1}$ for the OVII triplet. However, due to the large uncertainties, further higher S/N observations are required in order to accurately determine the redshift and, possibly, to analyze any line modulation with the spin/orbital period of DW Cnc.

3 DISCUSSION AND RESULTS

DW Cancrini is a variable binary classified as a CV from its Balmer emission lines (Stepanian 1982; Kopylov et al. 1988). The source was intensively studied in the optical band and periods of ≈ 38 , ≈ 86 and ≈ 69 minutes (see, e.g., Uemura 2002; Rodriguez-Gil et al. 2004; Patterson et al. 2004) were identified and explained as the WD spin period, the orbital period and spin-orbit beat, respectively.

Nevertheless, as suggested by Patterson et al. (2004), a confirmation of the DW Cnc spin period in the X-rays was necessary. Hence, analyzing the 0.3–10 keV data acquired by the XMM-Newton telescope, we have shown the existence of a 37.7 ± 4.5 minute periodicity consistent with the spin period of the white dwarf thus allowing us to classify DW Cnc a member of the intermediate polar class. The timing analysis reveals powers at harmonics of the white dwarf period, i.e. $P_{\text{spin}}/2 \approx 19$ minutes and $P_{\text{spin}}/3 \approx 14$

Table 2. Line parameters as measured from the RGS 1 and RGS 2 spectra of DW Cnc. The expected centroid wavelength in the rest-frame are extracted from the CHIANTI database (Dere 2001).

Line ID	$\lambda_{exp}(\text{\AA})$	$\lambda_{obs}(\text{\AA})$	Flux($\times 10^{14}$ erg s $^{-1}$ cm $^{-2}$)	ΔC	R	L	G
OVIII Ly- α	18.969	$18.966^{+0.009}_{-0.012}$	$13.6^{+0.1}_{-0.1}$	16	—	—	—
OVII (r)	21.600	$21.632^{+0.016}_{-0.008}$	$5.5^{+3.2}_{-2.9}$	14	$\lesssim 1$	$\lesssim 1.5$	$\lesssim 5$
OVII (i)	21.790	$21.835^{+0.019}_{-0.008}$	$8.1^{+4.7}_{-4.6}$	—	—	—	—
OVII (f)	22.101	$22.135^{+0.019}_{-0.008}$	$3.0^{+3.4}_{-2.6}$	—	—	—	—

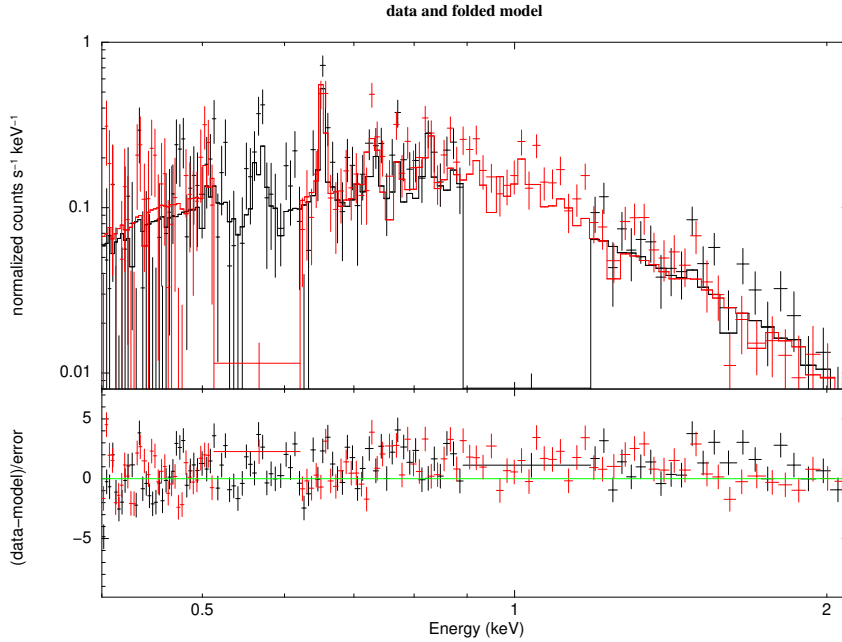


Figure 5. The best fit model superimposed on the RGS 1 (red) and RGS 2 (black) data. Note the presence a strong OVIII Ly- α line at 18.96 Å and the OVII He-like triplet.

minutes, being the second feature more evident. Unfortunately, the duration of the X-ray light curve limited our capability to have any clear detection of the orbital and spin-orbit beat periodicity corresponding to the frequency $\omega_{spin} - \omega_{orb} = 2\pi/P_{spin} - 2\pi/P_{orb}$. However, a sideband at the beat period ≈ 26 minutes possibly exists as originating from a $2\omega_{orb}$ modulation which could produce a feature at frequency $\omega_{spin} + \omega_{orb} = 2\pi/P_{spin} + 2\pi/P_{orb}$.

Note finally that the OM data in the UVM2 filter covers a total length of ≈ 146.6 minutes thus allowing us to identify a period of 75 ± 21 minutes which, within the quoted uncertainty, is consistent with both the 69 and 86 minute features reported in literature.

We also performed a spectral analysis of the phase average spectrum finding that the EPIC data can be described by a multi-temperature plasma model simply absorbed by the galactic neutral hydrogen column density. In particular, the best fit converged towards the values ($\chi^2 = 1.04$ for 540 d.o.f.) $nH = (3.1 \pm 0.3) \times 10^{20}$ cm $^{-2}$, $kT_{max} = 31^{+5}_{-4}$ keV, $\alpha = 0.65^{+0.06}_{-0.05}$, and $A_Z = 0.9^{+0.1}_{-0.1}$, respectively which corresponds the unabsorbed 0.3–10 keV band flux of $F_{0.3-10keV}^{una} = (1.68^{+0.02}_{-0.02}) \times 10^{-11}$ ergs $^{-1}$ cm $^{-2}$. When assuming a distance of ≈ 208 pc, the measured luminosity turns out to be $\approx 8.7 \times 10^{31}$ ergs $^{-1}$.

The best fit model provides an adequate description of the RGS spectra (< 0.3 keV) as well. In addition, in the low energy data, we noted the existence of a few emission lines (corresponding to the OVIII Ly- α transition and the OVII He-like triplet) which give us an hint that a photoionization mechanism is acting. In particular, the estimated large (small) values of the G (R) ratios (associated to the the OVII He-like triplet) suggests photonization and, since R decreases with increasing values of the electron density n_e , a lower limit on the electron density of $\approx 10^{11}$ cm $^{-3}$ (Porquet & Dubau 2000).

We note here that, since XMM-Newton data extends only up to ≈ 10 keV, a plasma temperature as large as $kT \approx 31$ keV (corresponding to the harder part of the *mekal* components embedded in the *cvmekal* model used here) could be un-reliable (but not different from other similar findings as in the case of PQ Gem (Evans et al. 2006)) and possibly arising from the usage of a multi-temperature model. Of course, further spectral observations extended to larger energies would allow to solve this issue.

We also remind that the spectral properties extracted in the phase intervals associated to the maxima and the minima of the source activity remain consistent (within the errors) with the values derived for the phase averaged spec-

trum. This fact, together with the absence of any evidence of a local partial covering, push us in interpreting the observed variability as due to aspect changes of the X-ray emitting region as the WD rotates. Also in this case, further and longer X-ray and/or optical observations are required in order to check the existence of periods other than that associated to the white dwarf spin in the DW Cnc data. High energy band X-ray data (see e.g. Landi et al. 2009) would also allow to firmly establish the spectral properties of DW Cnc.

ACKNOWLEDGEMENTS

This paper is based on observations from XMM-Newton, an ESA science mission with instruments and contributions directly funded by ESA Member States and NASA. We thank the anonymous Referee for the suggestions that greatly improved the paper. We thank for partial support the INFN projects TAsP and EUCLID. We warmly acknowledge Berlinda Maiolo, Sara Nucita, and Matteo Nucita for reading the manuscript. We warmly acknowledge ESAC (ESA) for the facilities provided.

REFERENCES

- A. G. A. Brown, A. Vallenari, T. Prusti, J. H. J. de Bruijne, et al. A&A, 2018
- Balman, S., 2011, ApJ, 741, 84
- Belanger, G., 2016, ApJ, 822, 14
- Bernardini, F., et al., 2017, MNRAS, 470, 4815B
- Cash, W. 1979, ApJ, 228, 939
- Dere, K. P., 2001, ApJSS, 134, 331
- de Martino, D., Matt, G., Belloni, T., Haberl, F., & Mukai, K., 2004, A&A, 415, 1009D
- de Martino, D., et al., 2005, A&A, 437, 935D
- Evans, P.A., & Hellier, C., 2004, MNRAS, 353, 447
- Evans, P.A., Hellier, C., Ramsay, G., & Cropper, M., 2004, MNRAS, 349, 715
- Evans, P.A., & Hellier, C., 2005, MNRAS, 359, 1531
- Evans, P.A., Hellier, C., & Cropper, M., 2006, MNRAS, 369, 1229
- Evans, P.A., & Hellier, C., 2007, ApJ, 663, 1277
- Haberl, F., 2002, in *The Physics of Cataclysmic Variables and Related Objects*, ASP Conference Proceedings, Vol. 261. Eds. B. T. Gänsicke, K. Beuermann, & K. Reinsch
- Hellier, C., Cropper, M., & Mason, K.O., 1991, MNRAS, 248, 233
- Hoard, D.W., et al., 2010, AJ, 140, 1313
- Kalberla, P. M. W., et al. 2005, A&A, 440, 775
- Kopylov, I. M., et al. 1988, Astrofizika, 28, 287
- Kuulkers, E., Norton, A., Schwope, A., & Warner B., 2006, in *Compact Stellar X-ray Sources*, ed. W. H. G., Lewin, & M., van der Klis, Cambridge Astrophys. Ser., 39, 421
- Landi, R., et al., 2009, MNRAS, 392, 630
- Mewe, R., Gronenschild, E. H. B. M., & van den Oord, G. H. J., 1985, A&AS, 62, 197
- Mukai, K., Ishida, M., & Osborne, J.P., 1994, PASJ, 46, L87
- Mukai, K., 2005, in *The Astrophysics of Cataclysmic Variables and Related Objects*, Proceedings of ASP Conference Vol. 330. Edited by J.-M. Hameury and J.-P. Lasota. San Francisco: Astronomical Society of the Pacific, p.147
- Mukai, K., Rana, V., Bernardini, F., & de Martino, D., 2015, ApJ, 807L, 30M
- Mukai, K., 2017, PASP, 2017, 129
- Norton, A.J., Beardmore, A.P., & Taylor, P., 1996, 280, 3, 937
- Nucita, A.A., et al., 2009, New Ast, 14, 302N
- Nucita, A.A., et al., 2009, A&A, 504, 973N
- Nucita, A.A., et al., 2011, A&A, 536, 75N
- Nucita, A.A., et al., 2014, A&A, 566, A121
- Nucita, A.A., et al., 2010, A&A, 515, A47
- Patterson, J., et al., 2004, PASP, 116, 516
- Parker, T.L., Norton, A.J., & Mukai, K., A&A, 439, 213
- Porquet, D., & Dubau, J. 2000, A&AS, 143, 495
- Ramsay, G., et al., 2004, MNRAS, 350, 1373
- Rodriguez-Gil, P., Gaensicke, B. T., Araujo-Betancor, S., & Casares, J. 2004, MNRAS, 349, 367
- Scargle, J. D. 1982, ApJ, 263, 835
- Szkody, P., et al., 2004, AJ, 128, 2443S
- Stepanian, J. A., 1982, Perem. Zvezdy, 21, 691
- Uemura, Y., et al. 2002, PASJ, 54, 299
- van Teeseling, A., Beuermann, K., & Verbunt, F., 1996, A&A, 315, 467

This paper has been typeset from a \LaTeX file prepared by the author.